Radiocarbon, Vol 61, Nr 5, 2019, p 1265–1291 DOI:10.1017/RDC.2019.42
Selected Papers from the 23rd International Radiocarbon Conference, Trondheim, Norway, 17–22 June, 2018

THE INFLUENCE OF CALIBRATION CURVE CONSTRUCTION AND COMPOSITION ON THE ACCURACY AND PRECISION OF RADIOCARBON WIGGLE-MATCHING OF TREE RINGS, ILLUSTRATED BY SOUTHERN HEMISPHERE ATMOSPHERIC DATA SETS FROM AD 1500–1950

Alan G Hogg[1]* • Timothy J Heaton[2] • Christopher Bronk Ramsey[3] • Gretel Boswijk[4] • Jonathan G Palmer[5] • Chris S M Turney[5] • John Southon[6] • Warren Gumbley[7]

[1]Waikato Radiocarbon Laboratory, University of Waikato, Private Bag 3105, Hamilton, New Zealand
[2]School of Mathematics and Statistics, University of Sheffield, United Kingdom
[3]Research Laboratory for Archaeology and the History of Art, University of Oxford, Oxford OX1 3QY, United Kingdom
[4]School of Environment, University of Auckland, New Zealand
[5]Palaeontology, Geobiology and Earth Archives Research Centre and ARC Centre of Excellence in Australian Biodiversity and Heritage, School of Biological, Earth and Environmental Sciences, University of New South Wales, Sydney, NSW 2052, Australia
[6]Department of Earth System Science, University of California, Irvine, CA 92697-3100, USA
[7]Department of Archaeology and Natural History, Australian National University, Canberra, Australia

ABSTRACT. This research investigates two factors influencing the ability of tree-ring data to provide accurate ^{14}C calibration information: the fitness and rigor of the statistical model used to combine the data into a curve; and the accuracy, precision and reproducibility of the component ^{14}C data sets. It presents a new Bayesian spline method for calibration curve construction and tests it on extant and new Southern Hemisphere (SH) data sets (also examining their dendrochronology and pretreatment) for the post-Little Ice Age (LIA) interval AD 1500–1950. The new method of construction allows calculation of component data offsets, permitting identification of laboratory and geographic biases. Application of the new method to the 10 suitable SH ^{14}C data sets suggests that individual offset ranges for component data sets appear to be in the region of ± 10 yr. Data sets with individual offsets larger than this need to be carefully assessed before selection for calibration purposes. We identify a potential geographical offset associated with the Southern Ocean (high latitude) Campbell Island data. We test the new methodology for wiggle-matching short tree-ring sequences and use an OxCal simulation to assess the likely precision obtainable by wiggle-matching in the post-LIA interval.

KEYWORDS: carbon dating of tree rings, radiocarbon calibration, radiocarbon wiggle-matching, SHCal13, Southern Hemisphere radiocarbon calibration.

INTRODUCTION

The conversion of terrestrial radiocarbon (^{14}C) ages into sidereal time requires appropriate calibration curves derived from absolutely dated archives that accurately reflect past atmospheric ^{14}C levels. Tree rings form the gold standard if obtained from well-replicated and dendrochronologically securely dated trees (Reimer et al. 2013a). Other archives, although forming an essential and highly valuable contribution to the current calibration curves, require various assumptions, potentially diminishing their reliability. For example, plant macrofossils contained within lake deposits (e.g. Lake Suigetsu) may experience variable residence times before incorporation into sediments, while also being susceptible to contamination because of their relatively small sample size (Bronk Ramsey et al. 2012); atmospheric ^{14}C concentrations derived from speleothems require us to make modeling assumptions about the dead carbon fraction (Southon et al. 2012); and the accuracy of reservoir-corrected surface marine ^{14}C dates can be compromised by variable marine reservoir ages (Reimer et al. 2013b).

*Corresponding author. Email: alan.hogg@waikato.ac.nz.

Four main factors, discussed more fully below, influence the ability of tree-ring data to provide accurate ^{14}C calibration: differences in atmospheric ^{14}C levels within the global atmosphere; the difference in timing of growing seasons; the accuracy, precision and reproducibility of the component ^{14}C data sets; and finally, the fitness and rigor of the statistical model used to combine the data into a curve.

Although the precision of the calibrated age associated with a single radiocarbon determination is influenced by the accuracy and reproducibility of component data sets, it is largely dominated by the structure of the calibration curve. Crucially, the variability observed in the calibration curve arises from non-linearity in atmospheric ^{14}C production, due to varying solar activity and geomagnetic field strength modifying impinging cosmic radiation levels, and changes in the global carbon cycle. Lengthy periods of declining ^{14}C production, matching the rate of radiocarbon decay, result in ^{14}C plateaux which turn precise radiocarbon measurements into extended calendar age ranges. For example, a carbon date of 2470 ± 20 BP in the center of the De Vries perturbation IIIb (Taylor and Bar-Yosef 2014: Figure 2.12a) translates into a 2-sigma calendar age range spanning ~275 yr (2715–2440 cal BP).

This inherent variability in atmospheric ^{14}C concentration is exploited by the technique known as "wiggle-matching," which refers to the Bayesian process of fitting several ^{14}C determinations which have unknown absolute calendar ages, but known relative age spacing (e.g. tree rings), to a ^{14}C calibration curve. Matching of the radiocarbon dates to the wiggles in the curve can not only significantly improve the precision of the age estimates (Galimberti et al. 2004) but also reduces the influence of minor offsets (Bronk Ramsey et al. 2001).

Many studies have benefitted from highly precise calendar ages obtained by wiggle-matching. These include the dating of critical tephra marker beds (e.g. Santorini (Manning et al. 2014), Taupo tephra (Hogg et al. 2012), locking in floating tree-ring ^{14}C sequences for calibration purposes (e.g. Hogg et al. 2016) and archaeological applications (e.g. Hogg et al. 2017; Palmer et al. 2014 and many others).

Radiocarbon wiggle-matching of short tree-ring series can, however, be problematic. Bayliss et al. (2017) ran a series of short (25–35 ring) wiggle-matches from longer, dendrochronologically dated, Medieval period oak sequences and compared the 95% highest posterior density (HPD) credible intervals for their calibrated calendar ages against the known dendrochronological age. To correspond to their nominal coverage, one would expect approximately 95% of these credible intervals to have included the true age. However Bayliss et al. (2017) found that just under half (47.7%) of the short wiggle-matches produced did not; and even 3 of the 5 long (120–207 ring) wiggle-matches were inaccurate.

Several possible reasons for such low coverage have been suggested. It may be that there are high levels of annual ^{14}C variation which are not currently captured by the calibration curve as they are not identifiable from the blocked[1] decadal, or bidecadal, data used in its construction. Such hidden annual variations have the potential to shift a wiggle-match by a considerable margin (see e.g. Pearson et al. 2018). However alternatively, and arguably more easily remedied, it may be that there are additional sources of variation present in the data—such

[1]The term "blocking" refers to formation of blocks of multiple tree rings.

https://doi.org/10.1017/RDC.2019.42 Published online by Cambridge University Press

as geographic offsets, seasonal effects, or laboratory biases—that are not suitably recognized and accounted for within the existing modeling of ^{14}C datasets.

The recent trend of collecting large numbers of high resolution (often annual) tree-ring calibration data exposes a calibration curve to a severe risk of bias if the high-resolution measurements are made from geographically restricted areas and/or seasonally biased records. With or without decadal measurements, high resolution data have the potential to swamp other data and so it is essential that steps are taken to model the data appropriately to mitigate these risks. There is an important question that needs to be answered: how do we incorporate high resolution tree-ring ^{14}C data into calibration curves, with the inherent risk of laboratory/geographical/seasonal bias potentially skewing the calibration curve? The current explosion of annual tree-ring accelerator mass spectrometry (AMS) analyses make this a pressing issue.

In this paper we investigate the potential presence of such additional variability (offsets/biases) in tree-ring ^{14}C data and the effect it can have on calibration. We utilize post-Little Ice Age (LIA) AD 1500–1950 extant and new Southern Hemisphere calibration ^{14}C data to study the sizes of such potential offsets across both location and laboratory; and introduce a new Bayesian method for curve construction, which permits each dataset to have an unknown offset from the others—potentially a laboratory, tree, or location effect. This method can adaptively estimate and incorporate possible offsets when both combining the individual calibration data into a curve and also the calibration of a new determination. Furthermore, our approach is able to identify any calibration sets which appear to have particularly large offsets in comparison to the other data. These sets can then be carefully considered and investigated further to assess their appropriateness for inclusion or otherwise. We identify one dataset which appears to have a significant offset that we discuss further for suitability for incorporating into a mid-latitude calibration curve. We compare and contrast SHCal13 compiled using a random walk model (RWM) with the curve constructed by this new approach and discuss its general suitability for international calibration. The combined impact of the new SH data sets and approach to calibration curve construction on wiggle-matching short sequences, is assessed by wiggle-matching a ^{14}C data set derived from a 60-ring palisade post, obtained from Otāhau Pā, the first New Zealand Māori pā (fort) to be precisely dated (Hogg et al. 2017). We also assess the impact of variable atmospheric radiocarbon levels on wiggle-matching short tree-ring sequences in the post-LIA interval by conducting a large number of simulations using the Bayesian calibration program OxCal (Bronk Ramsey et al. 2001; Bronk Ramsey 2009).

FACTORS INFLUENCING CALIBRATION ACCURACY

Currently only two atmospheric ^{14}C reservoirs are recognized for pre-AD 1950 material, with terrestrial samples calibrated using either Northern Hemisphere (NH, IntCal) or Southern Hemisphere (SH, SHCal) calibration curves. The ability of an atmospheric calibration curve to supply accurate calendar age information for dates derived from samples from a specific locality is influenced by four factors:

1. Differences in atmospheric ^{14}C levels within each of the two reservoirs (intra-hemispheric homogeneity), which may vary with time;
2. The difference in timing of growing seasons;
3. The accuracy, precision and reproducibility of component data sets; and

https://doi.org/10.1017/RDC.2019.42 Published online by Cambridge University Press

4. The suitability of the statistical approach that combines the component ^{14}C data sets into the calibration curve, and the linked approach used to calibrate a new determination against it.

Intra-Hemispheric and Inter-Hemispheric Offsets

An inter-hemispheric North/South (N/S) ^{14}C offset (e.g. 44 ± 17 yr for the time interval 195 BC to AD 1845; Hogg et al. 2011), probably resulting from a higher sea-air $^{14}CO_2$ flux from the larger expanse of SH oceans (Rodgers et al. 2011), is now well established (Hogg et al. 2013a). Braziunas et al. (1995) developed a three-dimensional global circulation model (GCM), which described atmospheric ^{14}C contours in response to oceanic boundary conditions. The model predicted a decline of atmospheric $\Delta^{14}C$ of 1‰ (~8 ^{14}C yr) per 10° of latitude, to a maximum of 5‰ between 50°N and 50°S. Although intra-hemispheric (regional) offsets have been claimed in numerous studies (e.g. in Japan, Nakamura et al. 2013 and Korea, Hong et al. 2013), unambiguous evidence for these offsets has remained elusive. Most importantly of all, a lack of quasi-simultaneous analysis of contemporaneous local/calibration curve sample pairs has hindered distinguishing regional from laboratory analytic offsets. To address this issue, McCormac et al. (1995) analyzed 9 sample pairs of dendrochronologically secure bristlecone pine and Irish oak for the interval 500–320 BC and found a mean offset of –41 ± 9.2 ^{14}C yr. Of the three suggested reasons for the offset (regional differences, wood pretreatment and dendrochronological issues), the authors concluded that published data reveal evidence for small location dependant (and possibly time varying) differences, which may be important for high precision wiggle-matching. Intensities of the high energy AD 775 ^{14}C spike have recently been measured in tree rings from Japan, California, Siberia, Poland, Germany, and New Zealand (Park et al. 2017). All NH measurements show statistically similar intensities, with the New Zealand data ~6‰ lower (Park et al. 2017), consistent with the measured N/S offset. It should be noted that strictly speaking, IntCal and SHCal are mid-latitude curves (Reimer et al. 2013b; Hogg et al. 2013a).

The Difference in Timing of Growing Seasons

It is postulated that regional offsets could be linked to differences in the timing of growing seasons for plants, possibly as a result of variations in the seasonal flux of $^{14}CO_2$ from the stratosphere into the troposphere (Kromer et al. 2001; Manning et al. 2001, 2014). Although this mechanism is often cited for small (e.g. ~20 yr) offsets from IntCal, many of the studies (e.g. Dee et al. 2010; Manning et al. 2014) have not directly dated paired regional/IntCal samples. There is therefore always the possibility of analytic offsets, either connected with the analysing laboratory or with the datasets composing IntCal. The ideal way of establishing small regional offsets is by quasi-simultaneous counting (for radiometric labs) or measurement within the same wheel (for AMS labs). Unfortunately, this is rarely done and the question about the existence of measurable seasonal ^{14}C gradients is still open to debate.

The Accuracy, Precision and Reproducibility of Component Data Sets

Calibration curves utilize a compilation of data generated by different laboratories at different times and using different analytic approaches. Although international intercomparisons

https://doi.org/10.1017/RDC.2019.42 Published online by Cambridge University Press

suggest that radiocarbon laboratories are generally accurate and precise (e.g. Scott et al. 2017), more rigorous intercomparisons analyzing successive tree rings have shown that laboratory analytic offsets can exist (e.g. Hogg et al. 2013b). Accurate calibration is also dependent upon accurate, precise and reproducible component data sets. Three factors influencing the development of accurate and precise calibration datasets are dendrochronological reliability, efficiency of pretreatment processes to remove contaminating modern or background contamination, and the measurement method. Tree-ring series with weak dendrochronological linkages can result in serious calibration curve errors. For example, the beginning of the "absolute tree-ring chronology" (Friedrich et al. 2004) was revised from 12,410 cal BP to 12,325 cal BP (Hogg et al. 2013b; M. Friedrich, IntCal dendro-meeting in Zürich, August 2015) leaving significant errors in IntCal13 (Hogg et al. 2016). Wood pretreatment procedures can vary significantly and range from more rapid acid-base-acid (ABA) processes to intensive alpha-cellulose extraction. Pretreatment effectiveness is influenced by sample age, preservation environment, species and sample size and what is effective in one study may not be suitable for another. It is important the labs undertaking ^{14}C measurements for calibration purposes initially determine appropriate pretreatment methods (see Southon and Magana 2010; Capano et al. 2018 for examples). Furthermore, tree-ring ^{14}C measurements can be made by both AMS and radiometric methods, with both having their strengths and weaknesses. While AMS has considerable potential for high resolution single ring dating and is likely to revolutionize tree-ring radiocarbon calibration, the mg-sized samples are more susceptible to modern contamination, compared with high precision radiometric samples which are of the order of 1500 times larger.

Statistical Approaches for Curve Construction

The current calibration curves, IntCal13 and SHCal13, use a random walk model (RWM) approach (Niu et al. 2013) which was also used for IntCal09 and Marine09 (Blackwell and Buck 2008; Heaton et al. 2009). This approach considered the change in the radiocarbon age from one year to the next to vary according to a normal distribution (a random walk). For the tree-ring-based portion of the curve, it was assumed that there were no possible additional sources of uncertainty beyond that reported by the laboratory. All the tree-ring observations were thus modeled as:

$$X_i = \mu(\theta_i) + \epsilon_i,$$

where X_i is the observed radiocarbon age of a tree ring of known calendar age θ_i; $\mu(\theta)$ is the underlying calibration curve at calendar age θ_i; and $\epsilon_i \sim N\left(0, \sigma_i^2\right)$ the reported lab uncertainty.

This approach does not permit the possibility that any offsets (laboratory, geographical, genera, etc.) may exist between groups of data. However, it can be seen that there appear to be time periods (e.g. AD 1800–1950) where the raw data are more dispersed than such a model would suggest. Furthermore, the consequence of this model is that, as more data become available, even if they are more scattered or offset, the credible intervals of the estimated calibration curve will narrow and potentially lead to overly precise and inaccurate calibration of new determinations. This would likely further exacerbate the low credible interval coverage seen in Bayliss et al.'s (2017) wiggle-match study.

The above issues could be addressed within the RWM but the International Calibration Working Group (IntCal) has decided to no longer use this approach in future IntCal and SHCal upgrades. The RWM was extremely slow to run which both removed the

https://doi.org/10.1017/RDC.2019.42 Published online by Cambridge University Press

opportunity to investigate the effect of model assumptions or individual datasets; and made it difficult to assess convergence of the Markov Chain Monte Carlo (MCMC) used to fit the model. Instead, the new IntCal curves will utilize a Bayesian Spline approach which is computationally more efficient while still maintaining the required rigor and ability to incorporate the unique features of the calibration datasets from different sources (both tree and non-tree based).

We present this new approach in summary only here; and only for the known age tree-ring-based data. A full statistical explanation of the new Bayesian Spline methodology and its application to data with uncertain calendar ages will be given elsewhere (Heaton et al. 2019). However we do describe how potential offsets between data can be incorporated in curve construction.

NEW CURVE CONSTRUCTION METHODOLOGY

Basic Bayesian Splines

Rather than modeling evolution of the radiocarbon age over time, the planned Bayesian spline approach considers $\Delta^{14}C$ directly. Specifically, we model the atmospheric value of $\Delta^{14}C$ at time θ as,

$$\Delta^{14}C(\theta) = \sum_{i=1}^{K} \beta_i B_i(\theta)$$

where $B_i(\cdot)$ are B-spline basis functions at a pre-chosen, fixed set of knots and $\boldsymbol{\beta} = (\beta_1, \ldots, \beta_K)^T$ are the unknown basis coefficients that determine the curve. Curve construction then proceeds by trying to choose a balance between a curve that goes close to the observed determinations but is also not overly rough which would likely be overfitting the data.

We achieve this by first specifying a prior that penalizes over-variation in the level of $\Delta^{14}C$ over time,

$$\pi(\beta|\lambda) \propto \exp\left(-\gamma \int \{\Delta^{14}C''(\theta)\}^2 d\theta\right).$$

Here γ is a smoothing parameter that defines the trade-off between fidelity to the data; and variation in the level of atmospheric radiocarbon. By modeling the curve in $\Delta^{14}C$ this penalty on roughness is constructed in a domain where, before observing data, we might believe the curve would exhibit approximately similar roughness over its history. This prior has the effect that we will not introduce spurious wiggles to our estimated calibration curve where they are not supported by the data itself.

The posterior for the $\Delta^{14}C$ curve is then found by finding a compromise between this prior and goodness-of-fit to the observed calibration data. Due to the blocking and the uncertainties in the calendar ages of the older (>14kyr) objects used to construct IntCal, it is easiest to assess this goodness-of-fit in the $F^{14}C$ domain. For a determination that represents a block of n_i years, we model the observed corrected fraction modern F_i for each object as

$$F_i = \frac{1}{n_i} \sum_{j=0}^{n_i-1} F^{14}C(\theta_i + j) + \epsilon_i,$$

https://doi.org/10.1017/RDC.2019.42 Published online by Cambridge University Press

where $F^{14}C(\theta)$ is the transformation of the calibration $\Delta^{14}C$ curve at time θ and $\epsilon_i \sim N\left(0, \sigma_i^2\right)$ is the reported lab uncertainty. This rigorous and exact incorporation of blocking in the data was not done for IntCal13 and SHCal13.

We assess fidelity in the $F^{14}C$ domain, as opposed to the radiocarbon age scale used for the IntCal13 and ShCal13 methodologies, since observational uncertainties are symmetric in $F^{14}C$. Again this offers an advance on IntCal13 and SHCal13 since, in the radiocarbon age domain, as we progress further back in time, the uncertainties on the observed radiocarbon ages can become significantly asymmetric. See Heaton et al. (2019) for more details.

Including Offset Terms

To include the potential for offsets in the radiocarbon age shared by a particular data set we adjust our model so that X_i, the observed radiocarbon age of a tree-ring datum i, is considered as

$$X_i = \frac{1}{n_i}\sum_{j=0}^{n_i-1}\mu\left(\theta_i + j\right) + \zeta_{j(i)} + \eta_i$$

with $\zeta_{j(i)}$ the potential offset shared by all observations in the set j. This can be incorporated into our Bayesian Spline approach via adjusting our assessment of fidelity in the $F^{14}C$ domain to

$$F_i = \gamma_{j(i)}\left\{\frac{1}{n_i}\sum_{j=0}^{n_i-1}F^{14}C\left(\theta_i + j\right)\right\} + \epsilon_i,$$

with $\gamma_{j(i)} = e^{\zeta_{j(i)}/8033}$ the $F^{14}C$ domain multiplier that equates to an offset $\zeta_{j(i)}$ in the radiocarbon age.

We place a prior on the size of potential offset $\zeta_{j(i)} \sim N(0, \tau^2)$. For this study, we use a relatively uninformative prior by setting $\tau = 20$. In fitting the model we are provided with not only posterior estimates of the calibration curve (through the spline coefficients $\boldsymbol{\beta}$) but also the estimated offsets $\zeta_{j(i)}$ for each dataset.

Model Estimation

Estimation of both the curve and the offsets is performed via MCMC. Unlike the RWM which required updating the value of the calibration curve one year at a time, the Bayesian spline model described above can be estimated using Gibbs sampling where the entire curve is updated simultaneously along its entire history. This makes estimation and convergence much quicker. Note that in estimation we also place uninformative priors on the smoothing parameter λ and update this within the sampler (see Heaton et al. 2019 for further details).

Impact on Calibration and Wiggle-Matching

The inclusion of potential offsets in our modeling also has an impact upon calibration of either a new, unknown age, radiocarbon determination or a wiggle-match. If one considers there may be potential offsets in the datasets that make up the calibration curve, then one should also include the possibility that a new, undated determination may also be offset. In the case of a single determination, this is equivalent to using the prediction interval of the calibration curve (rather than the credible interval). In the case of a wiggle-match, it is equivalent to introducing a potential shift up/down to the undated object before judging the quality of curve fit. In OxCal terms this would be considered a Delta_R adjustment. For our illustrative wiggle-match of the Otāhau Pā palisade post we include such an adjustment

https://doi.org/10.1017/RDC.2019.42 Published online by Cambridge University Press

using both the OxCal Delta_R with a uniform prior $\zeta_{j(i)} \sim U[-20, 20]$; and the same prior for offset as in curve construction i.e. $\zeta_{j(i)} \sim N(0, \tau^2)$ with $\tau = 20$.

APPLICATION OF NEW METHODOLOGY

Example 1: Recreating SHCal13

To assess the new curve construction methodology and to evaluate SHCal13 data component offsets, we first built a new version of the calibration curve using the same five datasets as SHCal13 (see Table 1). Figure 1 shows individual data points together with the 1 sigma SHCal13 curve (SHCal13-RWM) and the new curve (SHCal-NEW).

SHCal13-NEW follows predominantly the same shape as SHCal13-RWM although it appears in some time periods (e.g. AD 1760–1800 and 1900–1920) that the SHCal13-NEW estimates shows higher inter-annual variation, as indicated by more highly attenuated peaks and troughs.

In the periods where the curve drops between AD 1680–1710 and 1800–1820, the SHCal-RWM mean estimate lies somewhat below the SHCal13-NEW mean estimate (although still within the 1-sigma SHCal13-NEW envelope). Here we are mainly dependent upon QL data to inform the value of the curve—any potential offset in this data will therefore introduce a bias to the curve unless we incorporate it in modeling. In regions where QL data overlaps with other data, QL lies consistently younger in comparison suggesting such a bias may exist. Unlike the RWM, the Bayesian Splines Offset approach allows the possibility of such a QL laboratory offset and permits the entire QL set to shift upwards to provide a better overall fit. Since the QL data are the largest data set throughout the period of study, the overall mean of SHCal-NEW is slightly older than SHCal-RWM. Between AD 1650–1820, the mean of SHCal-NEW is on average 6.3 yr older. Between AD 1825–1900 the mean new curve averages 1.3 yr older.

The credible intervals for the curve created using Bayesian splines (with potential offsets) are wider than that created with the RWM. The 1-sigma intervals for SHCal13-NEW predominantly contain the 1-sigma intervals for SHCal13-RWM. The Bayesian spline method generates a curve with an average uncertainty σ of 13.9 over this time period, compared with the RWM of 10.7. This is likely due to the additional uncertainty caused by the incorporation of potential offsets. The wider envelope on the SHCal13-NEW curve means that when calibrating a radiocarbon determination against it, the credible range for the object's unknown age will generally be wider than the interval obtained by calibrating against SHCal13-RWM, the latter we consider unrealistically precise.

The relative offsets estimated by the new curve compilation method range from –7.1 to +4.5 yr, see Table 2, with the QL and UB data sets negative and the Wk, PTA and OZ offsets positive. The total range between the posterior means of the offsets is 11.6 yr and the standard deviation is 5.6. Of particular interest are that data sets ID 2 and 3 (and 6 in Table 3 below) contain measurements made by the Wk and UB laboratories on splits of the same wood samples. These measurements are on trees from the same location and species, providing some indication of the potential sizes of offsets between laboratories. The posterior mean difference between the Wk and UB data sets for these common wood samples is 12.8 ± 3.9 yr (with Wk older).

https://doi.org/10.1017/RDC.2019.42 Published online by Cambridge University Press

Table 1 Summary of SHCal13 AD 1500–1950 tree-ring chronologies and data sets showing segment lengths (# rings) and number of analyses (N). QL: Quaternary Isotope Lab; Wk: Waikato University; UB: Queens University Belfast; PTA: Pretoria; OZ: ANSTO. GPC: gas proportional counting; HPLSC: high precision liquid scintillation counting; AMS: accelerator mass spectrometry.

ID	Location	Species/lat., long.	Time interval	# rings (av.)	N	Notes
1: QL	Tasmania,	*Lagarostrobos*	AD 1898–1948	1-10	158	McCormac et al. (2002)
	Australia	*franklinii*	(52–2 cal BP)	(2.8)	119	Stuiver and Braziunas
	Chile	42°S, 147°E	AD 1664.5–1848	1-5	31	(1998)
	Chile	*Nothofagus dombeyi*	(285.5–102 cal BP)	(2.4)		GPC
		54°S, 71°W	AD 1900–1945	3		ABA (1658–1889)
		Nothofagus pumilio	(50–5 cal BP)			solv. extr.$^{+}$ alpha-cellulose
		51°S, 73°W				(1664.5–1848)
2: Wk*	Takapari Forest	*Libocedrus bidwillii*	AD 1505–1715	10	22	Hogg et al. (2002)
	Park, NZ	40°04'S, 175°59'E	(445–235 cal BP)	(10)		HPLSC
						solv. extr.$^{+}$ alpha-cellulose
3: UB*	Hihitahi (H) &	*Libocedrus bidwillii*	H: AD 1725–1945	10	45	McCormac et al. (1998)
	Takapari (T) Forest	*H:* 39°32'S, 175°44'E	(225–5 cal BP)	(10)		Hogg et al. (2002)
	Park, NZ	T: 47°01'S, 167°42'E	T: AD 1445–1715			HPLSC
			(505–235 cal BP)			solv. extr.$^{+}$ alpha-cellulose
4: PTA	Cape Town,	Cape Town pine	AD 1835–1900	1-2	14	Vogel et al. (1993)
	South Africa	34°S, 19°E	(115–50 cal BP)	(1.1)		GPC
						ABA
5: OZ	Western Tasmania,	*Lagarostrobos franklinii*	AD 1625–1775	10	16	Hogg et al. (2013a)
	Australia	42°S, 145°E	(325–175 cal BP)	(10)		Hua et al. (2004)
						AMS
						alpha-cellulose

*Data sets 2 and 3 obtained from splits of the same wood samples.

$^{+}$"solv. extr." = solvent extracted.

Table 2 Relative offset data for SHCal13 tree rings from AD 1500–1950 by different laboratories (refer to Table 1). Offsets calculated by the SHCal13-NEW curve compilation method.

ID	Offset from mean (yr)	Offset error (yr)
1: QL	–5.1	8.1
2: Wk	3.3	8.8
3: UB	–7.1	8.3
4: PTA	4.5	8.9
5: OZ	4.1	9.3

Example 2: Inclusion of New Data and Outlier Identification

Our next illustration demonstrates the inclusion of six other SH data sets compiled since the release of SHCal13. Here we aim to highlight both how this influences the width of the curve's credible interval, and how the offsets estimated by the method can be used to flag potential outlying datasets for further investigation.

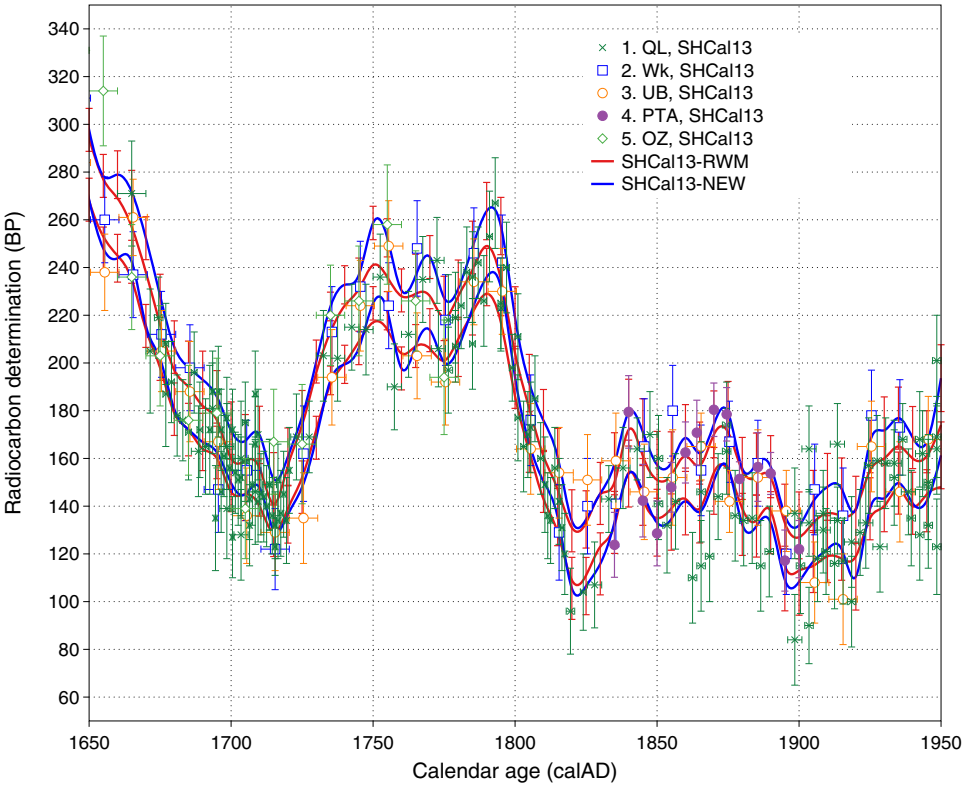

Figure 1 SHCal13 data sets 1–5, AD 1650–1950. Legend = Lab identifier, source of wood. SHCal13-RWM = SHCal13 curve as published, using the random walk model; SHCal13-NEW = new curve compiled using Bayesian splines with offsets, from SHCal13 data only. The Wk measurements from AD 1725-1935 are not shown as they were inadvertently left out of SHCal04 and SHCal13. The PTA AD 1850 value of 129 ± 14 yr BP as shown here and as given in the SHCal04 and SHCal13 data sets (http://intcal.qub.ac.uk/shcal13/query/) is incorrect: the value should be 155 ± 11 yr BP (corrected in Figure 3).

https://doi.org/10.1017/RDC.2019.42 Published online by Cambridge University Press

Table 3 Summary of new AD 1500–1950 SH tree-ring chronologies/data sets showing segment lengths (# rings) and number of analyses (N). HPLSC: high precision liquid scintillation counting; AMS: accelerator mass spectrometry.

ID	Location	Species/lat., long.	Time interval	# rings	N	Notes
6: Wk-Hihitahi	Hihitahi Forest Park, NZ	*Libocedrus bidwillii* 39°32'S, 175°44'E	AD 1725–1935 225–15 cal BP	10 (10)	22	McCormac et al. (1998) HPLSC solv. extr.$^{+}$ alpha-cellulose
7: Wk*-Hihitahi#	Hihitahi Forest Park, NZ	*Libocedrus bidwillii* 39°32'S, 175°44'E	AD 1705–1945 245–5 cal BP	10 (10)	45	Turney et al. (2016) AMS alpha-cellulose
8: Wk*-Doughboy^	Doughboy Bay, Stewart Isl., NZ	*Halocarpus biformis* 47°01'S, 167°42'E	AD 1705–1945 245–5 cal BP	10 (10)	45	Turney et al. (2016) AMS alpha-cellulose
9: Wk*-L. Tay^	Lake Tay, WA, Australia	*Callitris columellaris* 33°02'S, 120°45'E	AD 1705–1945 245–5 cal BP	10 (10)	45	Turney et al. (2016) AMS alpha-cellulose
10: Wk*-Campbell Isl.	Campbell Isl., NZ	*Dracophyllum longifolium* 52°31'S, 169°13'E	AD 1905–1945 45–5 cal BP	10 (10)	5	Turney et al. (2016) AMS alpha-cellulose
11: Wk-Auckland	Auckland, NZ	*Agathis australis*‡	AD 1652–1827 298–123 cal BP	5 (5)	72¶	Hogg et al. (2017) AMS solv. extr.$^{+}$ alpha-cellulose

Wk = samples analyzed at Waikato University for C. Turney.
^1915-1945 decades given preliminary multiple solvent (acetone) extractions.
¶duplicate analyses.
#1931–1950 decades from Takapari FP (40°04'S, 175°59'E).
+"solv. extr." = solvent (acetone) extracted.
‡kauri derived from the upper North Island of New Zealand but exact geographic location unknown.

Table 3 provides details of the tree-ring chronologies and ^{14}C data sets. To be suitable for calibration purposes, tree-ring ^{14}C data sets must be derived from a dendrochronologically securely dated piece of wood with appropriate wood pretreatment methods (Reimer et al. 2013a).

Dendrochronology

Set 6: Wk-Hihitahi (dendrochronology—L. Xiong, J. Palmer).

The New Zealand cedar (*Libocedrus bidwillii*) chronology network is well established and has been used for palaeoclimate reconstructions (Xiong and Palmer 2000a, 2000b; Palmer and Xiong 2004). The Hihitahi site is part of the network and consists of 49 crossdated trees spanning AD 1431–1991 with all the ring-width measurements lodged in the International Tree-ring Data Bank (ITRDB; newz066.rwl[2]). The specific tree selected for this study (H4702) was one of several dead trees found at the site and crossdated over the period AD 1456–1960 (505 yr). A site tree-ring chronology was compiled in the program COFECHA (Holmes 1983) from all the individual measurement series (after first being standardised to a mean of zero and standard deviation of 1.0). The selected tree had a Pearson correlation of 0.462 to the site chronology (once the series being tested had been removed from the master chronology; Grissino-Mayer 2001).

Set 7: Wk-Hihitahi (dendrochronology—L. Xiong, J. Palmer).*

The same tree (H4702) as previously used from Hihitahi (Set 6, above) was re-sampled for the time period AD 1701–1930. However, even though only a relatively small amount of wood was needed for the AMS dating there was insufficient remaining for the last two decadal samples (i.e. 1931–1950) (Turney et al. 2016). To complete the program we chose to use samples from a tree (TKP144) at another adjacent site (Takapari; ITRDB listing newz062.rwl). The Takapari site chronology covers AD 1256–1992 and the selected tree spans AD 1704–1989 with a Pearson correlation of 0.485 to the Takapari site master chronology.

Set 8: Wk-Doughboy (dendrochronology—J. Palmer).*

The pink pine (*Halocarpus biformis*) chronology from this site was originally developed by D'Arrigo et al. (1996) and updated in Palmer et al. (2015). The site chronology of 65 trees covers AD 1457–2010 (all measurements lodged on the ITRDB; newz118.rwl). The samples taken for radiocarbon dating were from a dead fallen tree (DBY225) that crossdated over the period AD 1620–1965 (346 yr) with a Pearson correlation of 0.597 to the master dating chronology (Turney et al. 2016).

Set 9: Wk-Lake Tay (dendrochronology—J. Palmer).*

The pioneering development of a chronology from *Callitris columellaris* from Lake Tay in southern Western Australia (Cullen and Grierson 2009) was recently updated with additional cores and cross-sections. This data is yet to be publicly available as more samples are currently being processed. Two different trees were used for the radiocarbon sample series—LTY14-37 for the period AD 1701–1800 and LTY14-05 for AD 1801–1950 (Turney et al. 2016). The first tree (LTY14-37) crossdated for 311 yr at AD 1630–1940 (Pearson correlation to the master series of 0.444) while the second tree (LTY14-05)

[2]https://www1.ncdc.noaa.gov/pub/data/paleo/treering/measurements/australia/newz066.rwl

https://doi.org/10.1017/RDC.2019.42 Published online by Cambridge University Press

crossdated for the shorter time period of AD 1790–2010 (221 yr) with a Pearson correlation of 0.557.

Set 10: Wk-Campbell Island (dendrochronology—J. Palmer).*

A 140-year chronology was produced from the small tree/shrub species *Dracophyllum longifolium* from the remote subantarctic Campbell Island (Turney et al. 2017; ITRDB listing newz117.rwl). The radiocarbon samples were taken from tree CMB05 that crossdated from AD 1900–2012 (Turney et al. 2016) and had a Pearson correlation to the master series of 0.392.

Set 11: Wk-Auckland (dendrochronology—G. Boswijk).

The kauri (*Agathis australis*) timber SPC002 (AD 1590–1849) used for dataset 11 was derived from one of seven cross-sectional slices obtained from large kauri beams that had been incorporated into the sub-floor structure of a 1930s transitional bungalow located on the grounds of St Pauls College, Richmond Road, Ponsonby, Auckland. All series were compared against each other using the crossdating program CROS73 (Baillie and Pilcher 1973) included in Dendro for Windows (Tyers 1997). All matches were checked using visual alignment of line graphs. SPC002 crossmatched with five timbers, with intra-site Baillie-Pilcher t-values (BPt) values ranging from 3.12 to 7.96 (mean T = 5.46; standard deviation [s.d.] = 1.80). SPC002 was calendar dated against a kauri master, and crosschecked against independent modern and archaeological chronologies (T values ranging from 3.36 to 9.58 [N = 14; mean T = 6.70; s.d. = 1.66]).

Pretreatment

Because tree-ring ^{14}C data has been collected from different species, it is important to pretreat the samples to a reliable wood fraction that reflects ambient atmospheric conditions at time of growth and is not affected by species-specific differences or variable lignin contents.

Pretreatment schemes for each data set are summarised in Table 3. Details for the solvent-extracted alpha-cellulose pretreatment for HPLSC are given in Hoper et al. (1998). In summary, wood is ground to pass a 20-mesh sieve, refluxed in Soxhlet apparatus using ethanol-chloroform, bleached with acidified $NaClO_2$ followed by a base/acid extraction. The AMS alpha-cellulose pretreatment (Turney et al. 2016) involves ABA/bleaching with acidified $NaClO_2$/ABA. Solvent extracted alpha-cellulose for AMS utilizes preliminary multiple acetone extractions to remove resins followed by the alpha-cellulose pretreatment described for AMS samples above.

Pretreatment Issues Connected with Resinous Wood Species

Despite many pretreatment studies finding resin removal by solvent extraction unnecessary (e.g. Vogel et al. 1986: 935, "it has been repeatedly shown that this organically soluble matter cannot influence the results noticeably"), and ABA pretreatment as effective as cellulose extraction (e.g. Capano et al. 2018), it is important that all tree species being utilized for calibration purposes be tested to demonstrate this. Two of the species (*Halocarpus biformis* and *Callitris columellaris*) utilized by Turney et al. (2016) are very resinous and inadequate removal of resins in samples close to the nuclear weapons testing ^{14}C boundary in age would have led to analytic errors if an initial solvent extraction preceding alpha-cellulose preparation was not utilized. Figure 2 shows ^{14}C ages with and without preliminary solvent extractions.

https://doi.org/10.1017/RDC.2019.42 Published online by Cambridge University Press

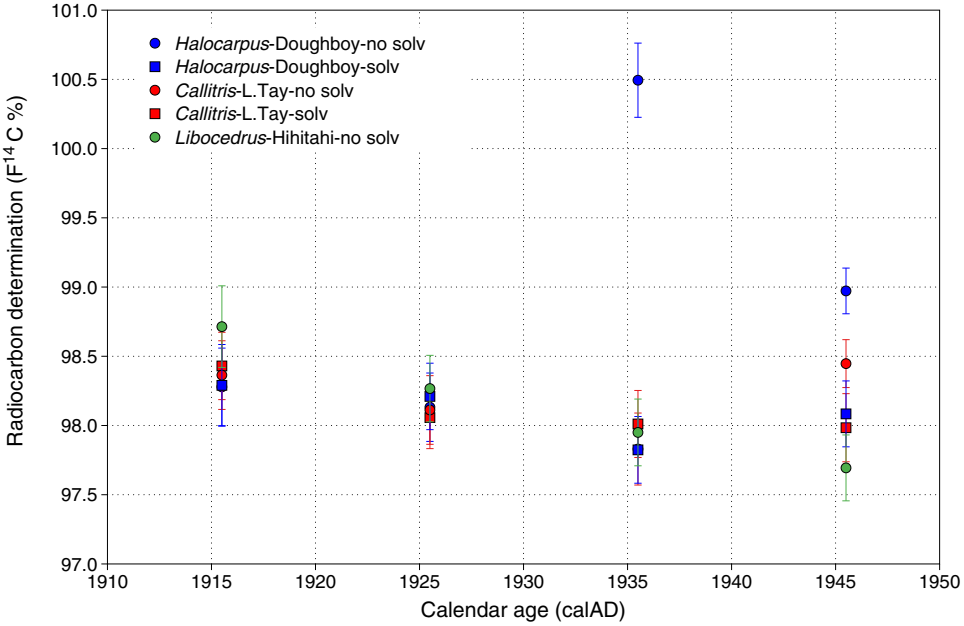

Figure 2 Doughboy Bay (*Halocarpus biformis*) and Lake Tay (*Callitris columellaris*) duplicate analyses with and without solvent pretreatment prior to alpha-cellulose extraction. Elevated ^{14}C levels due to nuclear weapons testing, peaking in the SH in 1965 (Turney et al. 2018), have been translocated by resins across earlier rings and only removed by a preliminary solvent extraction. Non-solvent extracted Wk*-Hihitahi analyses (*Libocedrus bidwillii*) are given for comparison.

An Initial Fit with RWM and Bayesian Splines

Individual data points are plotted in Figure 3 together with the 1 sigma SHCal13 curve (SHCal13-RWM) and the new curve (SH-All-NEW). Table 4 provides details of the relative offsets between the various data sets. We see that the majority of the new datasets have offsets that are of similar size to the offsets in the five sets used for SHCal13—with offsets in the region of –8 to 6 yr. However we clearly also identify an outlying dataset from Campbell Island with an estimated posterior mean offset of 22 ± 9 yr worthy of more detailed investigation. First however we briefly discuss each dataset in turn.

Data Set 6: Libocedrus bidwillii from Hihitahi, NZ.

Decadal measurements from NZ cedar sourced from Hihitahi State Forest Park were made by Waikato University using HPLSC and published in McCormac et al. (1998). This data set was inadvertently overlooked in the SHCal04 and SHCal13 iterations. The wood fraction dated was solvent extracted alpha-cellulose (see Hoper et al. 1998). The Wk-Hihitahi *L. bidwillii* data set has a mean offset of +5.7 ± 6.8 yr, which is broadly similar to the offset of Wk measurements in SHCal13 (+3.3 ± 8.8 yr—Table 2).

Data Sets 7, 8, 9, 10.

Decadal measurements from Hihitahi Forest Park (set 7), Doughboy Bay, Stewart Island, NZ (set 8), Lake Tay, Western Australia (set 9) and Campbell Island, NZ (set 10) were made by the Waikato AMS laboratory and published in Turney et al. (2016). The alpha-cellulose wood

https://doi.org/10.1017/RDC.2019.42 Published online by Cambridge University Press

Table 4 Relative offsets of all available SH tree-ring ^{14}C data sets (AD 1500–1950).

Data set	ID	Offset from mean (yr)	Offset error (yr)
1	QL	–7.7	5.7
2	Wk	2.8	7.0
3	UB	–8.1	6.1
4	PTA	6.8	6.6
5	OZ	2.8	7.6
6	Wk-Hihitahi	5.7	6.8
7	Wk*-Hihitahi	–6.2	6.6
8	Wk*-Doughboy	–0.8	6.8
9	Wk*-L. Tay	3.7	6.7
10	Wk*-Campbell Isl.	22.2	9.0
11	Wk-Auckland	1.7	5.8

fraction was dated with details of the pretreatment methods given in Turney et al. (2016). The youngest samples (i.e., AD 1940–1950) from the resin-rich Doughboy and Lake Tay sites were subject to an initial solvent extraction to remove mobile components (resins, etc.) translocating ^{14}C generated by atomic weapons testing across the ring boundaries.

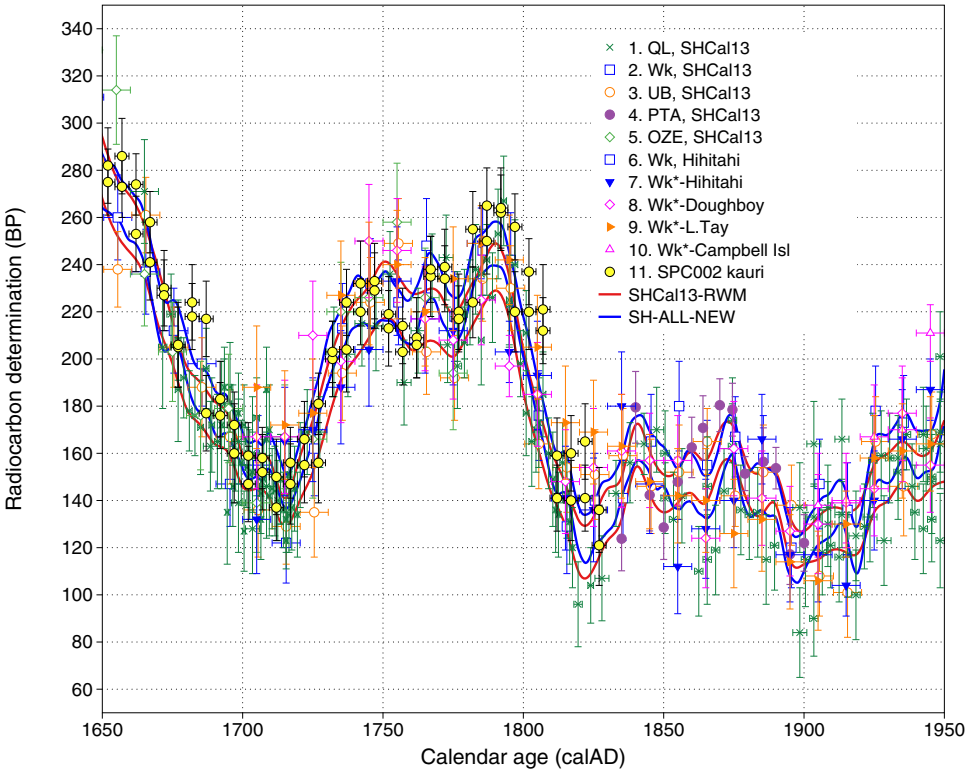

Figure 3 SHCal13 data sets 1–5, with new data sets, 6–11, AD 1650–1950. Legend = lab identifier, source of wood. Wk* = samples analyzed at Waikato University for C. Turney. SHCal13-RWM = SHCal13 curve as published; SHCal-All-NEW = new curve compiled from all 11 potential SH data sets. The correct PTA AD 1850 value of 155 ± 11yr BP is shown here.

https://doi.org/10.1017/RDC.2019.42 Published online by Cambridge University Press

The AMS data sets from Hihitahi, Doughboy Bay and Lake Tay broadly follow SHCal13 with mean offsets of –6.2 ± 6.6 yr, –0.8 ± 6.8 yr and 3.7 ± 6.7 yr respectively.

Although the Lake Tay offset of 3.7 ± 6.7 yr shows these data generally conform to the average of the other data sets, some of the measurements suggest the possibility of pre-AD 1950 resin translocation across ring boundaries. The decades centered on AD 1825 and 1875 for example, appear to be unusually offset from the mean SH-ALL-NEW curve. We re-analyzed these 2 data points with initial solvent extractions (Figure 4) and although the new results are not statistically different from the initial analyses, both solvent-extracted data points are more conformable. For the purposes of this paper, we have retained the Lake Tay data but further investigations into Lake Tay *Callitris columellaris* will be required before these data can be accepted for ^{14}C calibration purposes. The Campbell Island measurements have an offset of 22.2 ± 9.0 yr and are discussed in more detail below.

Data Set 11: Agathis australis from Auckland, NZ.

Replicate 5-ring segments of kauri were analyzed by the Waikato AMS laboratory for the interval AD 1650–1829. The data, previously shown in graphic form only in Hogg et al. (2017) are given in Table 5. All duplicated analyses are statistically consistent at the

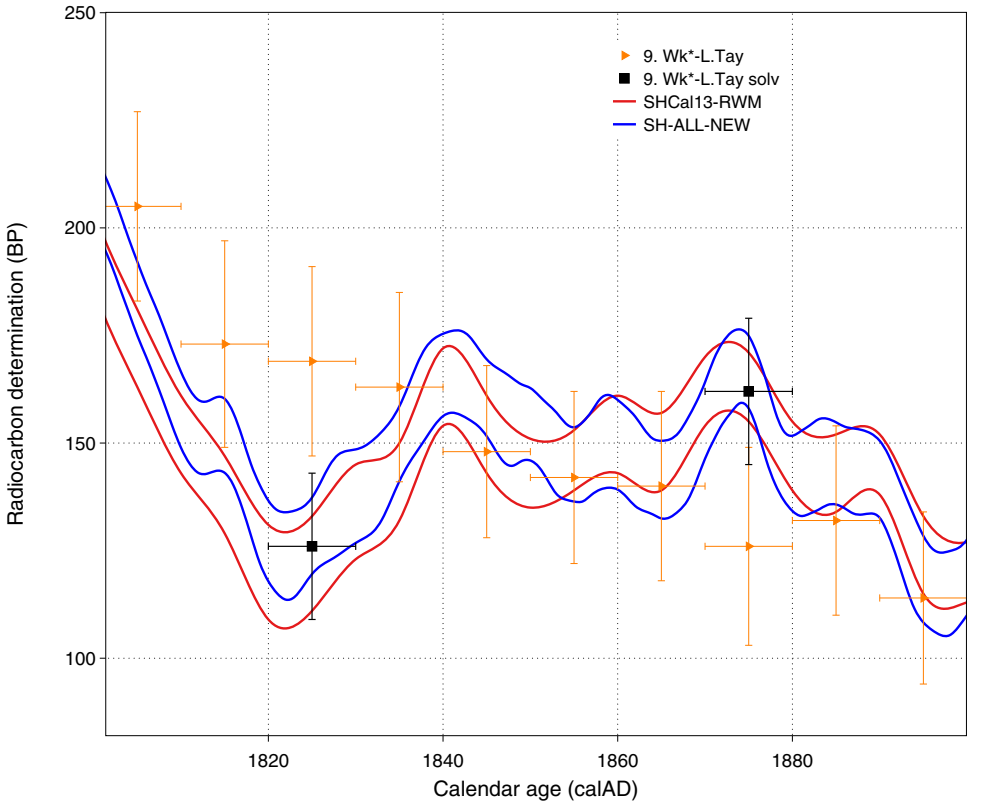

Figure 4 Lake Tay (Western Australia) AD 1825 and 1875 tree-ring ^{14}C analyses with and without solvent pretreatment prior to alpha-cellulose extraction. The solvent extracted values conform more closely to the SH-ALL-NEW curve suggesting the possibility of resin translocation across ring boundaries.

https://doi.org/10.1017/RDC.2019.42 Published online by Cambridge University Press

Table 5 *Agathis australis* tree-ring ^{14}C data—sample SPC002 (AD 1650–1829).

Mid-ring (AD)	Ring nr. (first–last) (AD)	Wk lab nr.	^{14}C age (yr BP ± 1σ)
1652	1650–1654	44145A	282 ± 16
1652	1650–1654	44145B	275 ± 14
1657	1655–1659	44146A	286 ± 16
1657	1655–1659	44146B	273 ± 13
1662	1660–1664	44147A	253 ± 16
1662	1660–1664	44147B	274 ± 13
1667	1665–1669	44148A	241 ± 16
1667	1665–1669	44148B	258 ± 13
1672	1670–1674	44149A	230 ± 16
1672	1670–1674	44149B	227 ± 15
1677	1675–1679	44150A	205 ± 17
1677	1675–1679	44150B	206 ± 18
1682	1680–1684	44151A	224 ± 16
1682	1680–1684	44151B	218 ± 14
1687	1685–1689	44152A	217 ± 16
1687	1685–1689	44152B	177 ± 16
1692	1690–1694	44153A	183 ± 16
1692	1690–1694	44153B	176 ± 14
1697	1695–1699	44154A	160 ± 21
1697	1695–1699	44154B	172 ± 14
1702	1700–1704	44155A	147 ± 16
1702	1700–1704	44155B	159 ± 14
1707	1705–1709	44156A	152 ± 16
1707	1705–1709	44156B	158 ± 13
1712	1710–1714	44157A	150 ± 16
1712	1710–1714	44157B	137 ± 14
1717	1715–1719	44158A	147 ± 17
1717	1715–1719	44158B	156 ± 15
1722	1720–1724	44159A	166 ± 16
1722	1720–1724	44159B	155 ± 16
1727	1725–1729	44160A	156 ± 17
1727	1725–1729	44160B	181 ± 13
1732	1730–1734	44161A	200 ± 16
1732	1730–1734	44161B	203 ± 13
1737	1735–1739	44162A	204 ± 18
1737	1735–1739	44162B	224 ± 14
1742	1740–1744	44163A	232 ± 18
1742	1740–1744	44163B	220 ± 14
1747	1745–1749	44164A	233 ± 16
1747	1745–1749	44164B	229 ± 16
1752	1750–1754	44165A	213 ± 16
1752	1750–1754	44165B	219 ± 16
1757	1755–1759	44166A	214 ± 16
1757	1755–1759	44166B	203 ± 14
1762	1760–1764	44167A	209 ± 17
1762	1760–1764	44167B	206 ± 14
1767	1765–1769	44168A	235 ± 17

https://doi.org/10.1017/RDC.2019.42 Published online by Cambridge University Press

Table 5 (*Continued*)

Mid-ring (AD)	Ring nr. (first–last) (AD)	Wk lab nr.	^{14}C age (yr BP ± 1σ)
1767	1765–1769	44168B	238 ± 14
1772	1770–1774	44169A	239 ± 16
1772	1770–1774	44169B	234 ± 14
1777	1775–1779	44170A	220 ± 16
1777	1775–1779	44170B	217 ± 14
1782	1780–1784	44171A	255 ± 16
1782	1780–1784	44171B	224 ± 15
1787	1785–1789	44172A	265 ± 16
1787	1785–1789	44172B	250 ± 14
1792	1790–1794	44173A	262 ± 16
1792	1790–1794	44173B	264 ± 17
1797	1795–1799	44174A	220 ± 17
1797	1795–1799	44174B	256 ± 14
1802	1800–1804	44175A	220 ± 16
1802	1800–1804	44175B	237 ± 14
1807	1805–1809	44176A	221 ± 19
1807	1805–1809	44176B	212 ± 14
1812	1810–1814	44177A	159 ± 16
1812	1810–1814	44177B	141 ± 14
1817	1815–1819	44178A	140 ± 17
1817	1815–1819	44178B	160 ± 16
1822	1820–1824	44179A	165 ± 16
1822	1820–1824	44179B	141 ± 14
1827	1825–1829	44180A	136 ± 18
1827	1825–1829	44180B	121 ± 17

5% significance levels (Ward and Wilson 1978). The data follow the shape of SHCal13 closely and have an offset to the mean of all 11 data sets of 1.7 ± 5.8 yr.

The SH calibration curve SHCal13 (Figure 1) contains three higher resolution QL South American *Nothofagus* data points centered on AD 1819.5 (3-ring), 1824 (2-ring), 1828 (5-ring). If the QL analyses had a systematic (perhaps temporal) offset towards younger ages, the high resolution data would have the potential to overly influence the calibration curve towards younger ages at this time. Because of the potential impact of this upon wiggle-matching short tree-ring sequences, we extended the 5-year kauri measurements to overlap with this period (Figure 5). The new kauri data centered on AD 1817, 1822, and 1827 are considerably older than the equivalent QL data, and are more comparable with measurements from the other data sets. The apparent QL offset appears to be analytic in nature. Unpublished South American *Fitzroya* decadal data (De Pol-Holtz pers. comm. 2018) centered on decades AD 1818.5 and 1828.5 are also older (Figure 5) suggesting a geographic offset at this time is unlikely.

Outlying Campbell Island—A Geographic Offset?

The estimated Campbell Island offset of 22.2 ± 9.0 yr clearly sets this dataset apart from the rest. However it is important not to simply discard data because they appear to be outlying but

https://doi.org/10.1017/RDC.2019.42 Published online by Cambridge University Press

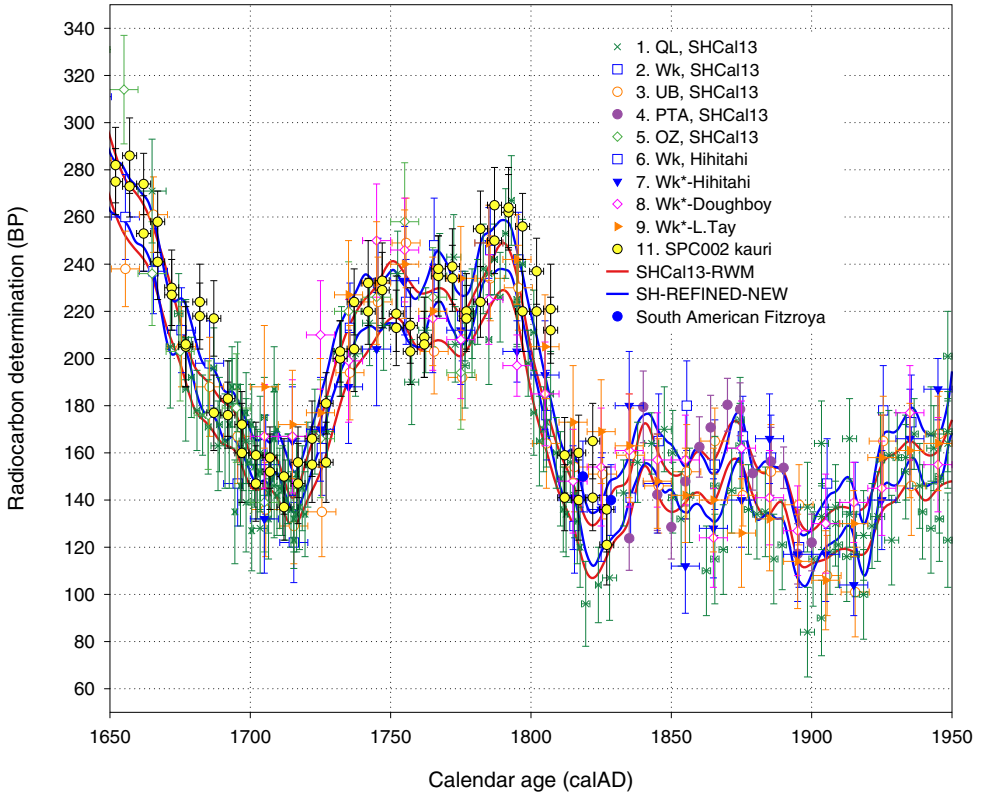

Figure 5 SH-REFINED-NEW calibration curve constructed from accepted data sets 1–9 and 11. SHCal13 curve given for comparison. The two decadal South American Fitzroya data points centered on AD 1818.5 and 1828.5 are courtesy of Dr Ricardo De Pol-Holz and have not been used in curve construction.

instead investigate the potential reasons behind such occurrences. Outliers may be genuine erroneous measurements in which case they should be removed; but alternatively they may represent genuine phenomena, in which case they should not only be kept but one should also think about what the implications of such real phenomena might be.

In our case, the Campbell Island, Hihitahi, Doughboy Bay, and Lake Tay samples were pretreated and graphitized as a group in the Waikato AMS laboratory, with the graphite samples measured in the same AMS wheel at the UCI Keck AMS laboratory. A large offset from any one of these 4 data sets is therefore unlikely to be analytic and more likely to be geographic in nature. As Campbell Island lies at 52°S amidst the Southern Ocean, the high ^{14}C ages (low ^{14}C concentration) probably result from dilution by outgassed old CO_2 associated with Southern Ocean upwelling (Turney et al. 2016). The ability to identify data sets with geographic biases is an important and innovative characteristic of this new method of curve construction.

In light of this, since we are aiming to provide a mid-latitude SHCal curve, we choose to discard Campbell Island from the calibration data. It should however provide a key note of caution for those wishing to calibrate data arising from locations adjacent to the Southern Ocean.

https://doi.org/10.1017/RDC.2019.42 Published online by Cambridge University Press

Construction of a New Southern Hemisphere Calibration Curve for the Interval AD 1500 1950

The new Bayesian Spline curve fitting regime described above has identified 10 suitable from 11 possible datasets for construction of a new SH calibration curve (SH-REFINED-NEW) for the interval AD 1500–1950, with the omission of data set 10 (Campbell Island) for the reasons given above. After a refitting of the Bayesian spline on these 10 datasets, the resultant calibration curve can be seen in Figure 5 with the relative offsets given in Table 6. The same figure (Figure 5) also shows the SHCal13-RWM published output using just the five datasets available in 2013.

Many of the features discussed in Example 1 (Recreating SHCal13) can again be seen when comparing the Bayesian spline SH-REFINED-NEW estimate (using the selected 10 datasets) against the SHCal13-RWM estimate (using just the five datasets). The Bayesian spline model and the addition of the new data sets do not change the overall shape of the curve significantly although peaks and troughs in the curve are more attenuated with SH-REFINED-NEW. The mean of SH-REFINED-NEW is still somewhat lower where the curve drops between AD 1680–1710 and 1800–1820, as a result of the curve in these regions being highly influenced by the QL data which, when compared to the rest of the data in this time period, seems to be consistently younger, suggesting a possible offset.

Importantly, despite the addition of the five new data sets, the width of the 1-sigma interval of SH-REFINED-NEW is still larger than the SHCal13-RWM estimate based on only five data sets. The average uncertainty σ for SH-REFINED-NEW is 12.2 over this time period, compared with the average SHCal13-RWM σ of 10.7. This suggests that offsets between datasets really are present in calibration data. As described earlier, there is evidence that the existing RWM can provide estimates that are overly precise which in turn leads to inaccurate calibration. Therefore a method that does not provide estimates with higher precision than the RWM, even after the inclusion of additional data which one might expect to increase precision, is probably desirable.

The total offset range for the refined curve is 14.9 yr, with a standard deviation of 5.5. These values are comparable with those values found for SHCal13 (SHCal13 range = 11.7 yr; s.d. = 5.6). Based on these findings, we suggest that new datasets with offsets lying

Table 6 Relative offsets of the 10 suitable SH tree-ring ^{14}C data sets (AD 1500–1950), combined to produce curve SH-REFINED-NEW.

Data set	ID	Offset from mean (yr)	Offset error (yr)
1	QL	–7.7	7.1
2	Wk	2.8	8.3
3	UB	–8.1	7.5
4	PTA	6.8	7.8
5	OZ	2.8	8.7
6	Wk-Hihitahi	5.6	7.8
7	Wk*-Hihitahi	–6.1	7.8
8	Wk*-Doughboy	–0.7	7.8
9	Wk*-L. Tay	3.7	7.9
11	Wk-Auckland	1.7	7.3

https://doi.org/10.1017/RDC.2019.42 Published online by Cambridge University Press

significantly outside these ranges (such as the Campbell Island data) be examined carefully but should not however be automatically excluded.

RADIOCARBON WIGGLE-MATCHING

Part of the motivation for determining the component offsets of suitable SH data sets was to investigate the accuracy of radiocarbon wiggle-matching in the AD 1500–1950 time range. We were primarily interested in two aspects of wiggle-matching short sequences: (1) the accuracy and precision of wiggle-matching using the new SH curve SH-REFINED-NEW compared with SHCal13; (2) using OxCal and SH-REFINED-NEW in a process of simulation to estimate the level of precision likely to be achieved when wiggle-matching short sequences, from archaeological material for example.

The inclusion of offsets in curve construction has consequences for calibration. If there are potential offsets in the datasets used to create the calibration curve, similar offsets should be considered to exist in any data set that we might calibrate—especially since the data going into the calibration curve is considered particularly high quality. We therefore need to incorporate such a potential offset for our undated sample when performing our calibration procedure. This will typically have the effect of widening the intervals of calibrated dates.

Comparison of SHCal13 and the New Curve SH-REFINED-NEW for Wiggle-Matching Short Sequences

To compare the effect of both the new curve methodology, and the incorporation of potential offsets, for wiggle-matching sequences with short segment lengths, we utilized a 60-ring (12 five-ring segments) *Prumnopitys ferruginea* (miro) palisade post ^{14}C data set obtained from Otāhau Pā, Taupiri, New Zealand (Hogg et al. 2017). We investigate both the effect on the wiggle-match when using the SHCal13 curve and SH-REFINED-NEW curve; and also when one does, or does not, recognize the possibility that the undated sample may also have an offset.

Inclusion of offsets in datasets during calibration can be done in OxCal via the Delta_R function (Bronk Ramsey 2009). OxCal however does not have the feature to incorporate the blocking present in the radiocarbon determinations of our palisade post, i.e. that each section of the post relates to the average of a 5-year segment and not just a single year. It also does not currently allow use of an annually resolved calibration curve (instead taking a subsampled output on a coarser 5-year grid). We therefore also include our own wiggle-match procedure that both permits us to use our annually resolved SH_REFINED_NEW curve fully; and also recognizes and includes the blocking in the palisade post when determining the wiggle-match.

We performed five comparison wiggle-matches:

Using SHCal13

i. OxCal with no incorporation of a possible offset in palisade post and no recognition of palisade blocking;
ii. OxCal with a potential palisade post offset modeled as Delta_R but no recognition of palisade blocking;Using SH-Refined-New

https://doi.org/10.1017/RDC.2019.42 Published online by Cambridge University Press

iii. OxCal with no incorporation of a possible offset in palisade post and no recognition of palisade blocking;

iv. OxCal with potential post offset modeled as Delta_R but no recognition of palisade blocking;

v. Personally coded approach using annually resolved calibration with both recognition of palisade blocking and potential post offset.

When using OxCal and including a potential miro palisade post offset, we applied the OxCal Reservoir Offset ("Delta_R") with a uniform prior of −20 to +20 yr (i.e. Delta_R("",U(−20,20)). All OxCal wiggle-matches also employed outlier analysis (Bronk Ramsey 2009) using Outlier_Model ("SSimple",N(0,2),0,"s") with {Outlier, 0.05} (which allows individual samples—roughly 1 in 20—to be outliers) to down-weight outliers. For wiggle match v) that incorporated fully the 5-year blocking within the wiggle-match, we modeled the potential offset term as $\zeta \sim N(0, 20^2)$ to mirror SH-REFINED-NEW's curve construction.

We report the estimated calendar age of the most recent (outermost) tree ring in the Miro post in Table 7 and graph the post's determinations against the two curves in Figure 6.

We note that this period of the calibration curve has a reverse and rapidly changing slope in the ~AD 1715–1750 interval (Figure 6). Because of this, and contrary to what is normally expected, the oldest ^{14}C miro post dates are associated with felling of the tree (outside rings—highest ring numbers), and the younger ^{14}C dates associated with the time of initial growth (center rings—lowest ring numbers).

It is likely this unique aspect of the miro post is the reason that little difference is seen between the calibrated age ranges for the different methods. Considering the effect of including offsets

Table 7 Summary of wiggle-matching New Zealand Prumnopitys ferruginea (miro) post 005 ^{14}C data against SHCal13 and SH-REFINED-NEW. Age estimates correspond to the most recent (outermost) tree ring in the post.

Curve	Analysis method	Calibrated mean age (cal AD ± 1σ)	Calibrated 95% prob. range (cal AD)	Estimated offset (yr)	Calibrated 95% prob. range span (yr)
SHCal13-RWM	OxCal (no block) No Delta_R	1769 ± 2	1765–1775	n.a.	10
SHCal13-RWM†	OxCal (no block) Delta_R(U(-20,20))	1770 ± 3	1765–1776	–2.5 ± 6.3	11
SH-REFINED-NEW†	OxCal (no block) Delta_R(U(-20,20))	1767 ± 2	1762–1772	–6.0 ± 6.0	10
SH-REFINED-NEW	OxCal (no block) No Delta_R	1766 ± 2	1762–1771	n.a.	9
SH-REFINED-NEW*	Annual (blocking)	1766 ± 2	1762–1771	See below	9

(† and *) These wiggle-matches included a potential offset ζ between the miro post and the calibration curve datasets. The OxCal wiggle-matches (†) utilize a uniform Delta_R prior Delta_R("Wk",U(−20,20)); the exact blocking (*) modeled the offset as $\zeta \sim N(0, 20^2)$ to match the curve construction. The code used for the exact blocking approach did not estimate ζ directly since it is not required to perform calibration.

https://doi.org/10.1017/RDC.2019.42 Published online by Cambridge University Press

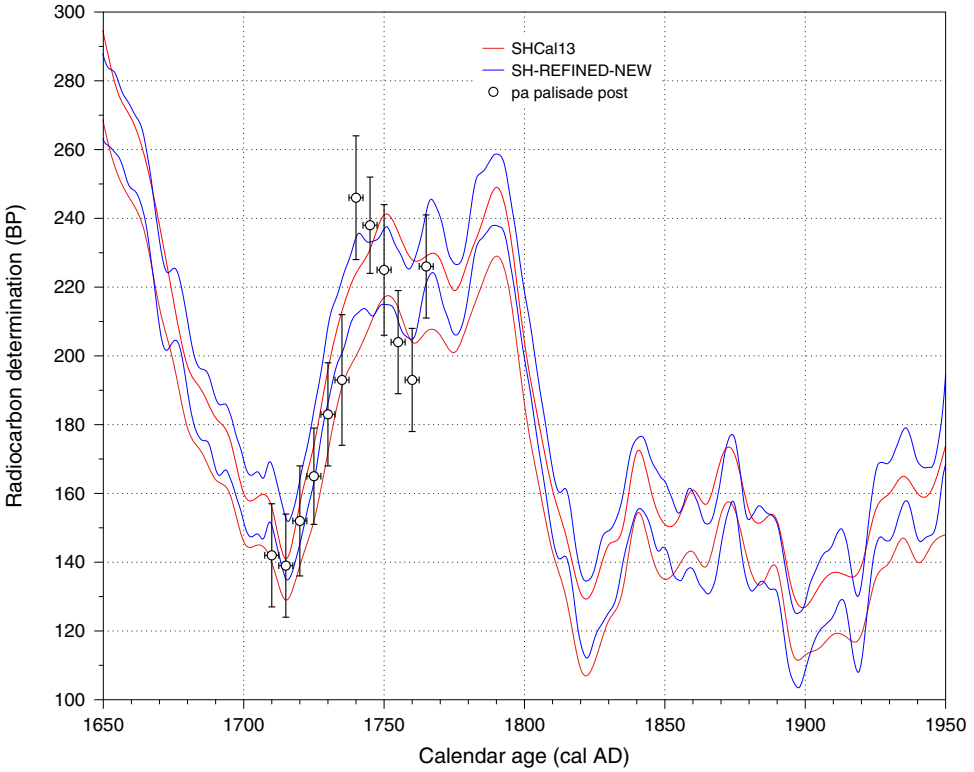

Figure 6 Unknown calendar-age ^{14}C results from the New Zealand *Prumnopitys ferruginea* (miro) palisade post 005 plotted against SHCal13 and SH-REFINED-NEW calibration curves.

on your undated sample when calibrating, for the miro post the wiggle-match can only fit well at one individual time period whether or not it is believed to be offset. However, the inclusion of possible offsets in data to be calibrated does have a much larger effect in general, and especially on single sample observations, where it serves to widen the credible intervals. Regarding the difference between the two curves, we do see some minor differences in the calibrated age ranges between the SHCal13 and SH-REFINED-NEW curves, with the SH-REFINED-NEW placing the tree slightly older albeit only by a few years.

Simulation of Probable Levels of Precision When Wiggle-Matching Short Sequences in the Interval AD 1500–1950

We used OxCal and our Bayesian spline annual curve (SH-REFINED-NEW) in a process of simulation to estimate the level of precision likely to be achieved when wiggle-matching short tree-ring sequences (as typically found in palisade posts) in the interval AD 1500–1950 (Figure 7). We undertook 10 simulations with end points every decade through this period. The coloured squares represent the average total 95% calibrated age range span (oldest cal BP date minus youngest cal BP date)—lower is better. The vertical axis "Number" shows how the 95% range span changes by increasing the number of radiocarbon determinations per wiggle-match, from a minimum of one (a single determination covering the entire 60-rings) to a maximum of 12 (i.e. 12 determinations of 5-ring blocks in a 60-ring palisade

https://doi.org/10.1017/RDC.2019.42 Published online by Cambridge University Press

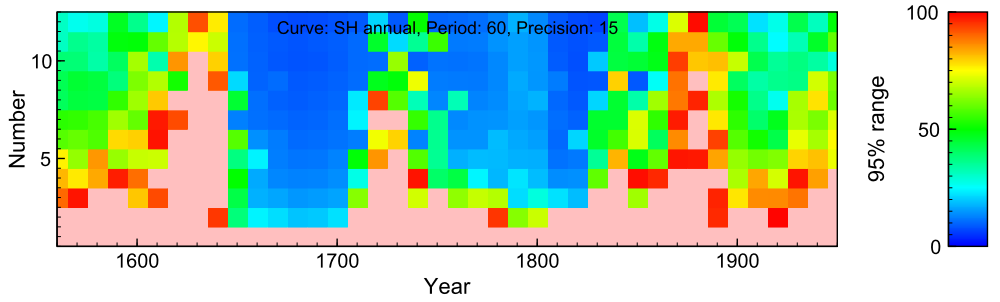

Figure 7 Average total 95% calibrated age range (oldest cal BP date minus youngest cal BP date) when wiggle-matching 60-ring segment lengths during the interval AD 1500–1950. Simulations using SH-REFINED-NEW calibration curve with segment length of 60 yr (rings). Precision (1σ error) = ± 15 ^{14}C yr. Large number of simulations often give multiple solutions, resulting in a high average range. Where there are repeating structures that could be confused, the average ranges are longer.

post). Using the example of the miro post wiggle-match discussed above, the Bayesian spline approach with SH-REFINED-NEW produced a range end date of AD 1766 and a total range span of 9 yr (Table 7). Figure 7 shows that a high level of precision such as this can be achieved with as few as five determinations per wiggle-match for time ranges with sufficient structure in the calibration curve (e.g. AD 1670–1700; AD 1760–1820). The simulations also show that 60-ring sequences may not be long enough to produce precise wiggle-matches for some time intervals, due to repeating structures (for example, AD 1620–1640, AD 1860–1890).

There is clear structure from the calibration curve SH-REFINED-NEW in Figure 7. For the New Zealand Otāhau Pā palisade post example the outermost youngest rings lie in a zone of highest available precision (dark blue 95% probability range span of <10 yr. The time period before AD 1650 is more problematic with a large ^{14}C plateaux influencing the interval ~AD 1450–1650 and resulting in probable ranges of 20–30 yr or more, even with a 60-ring wiggle-match containing 12 determinations. The very low precision (high ranges) associated with calendar ages younger than AD 1850 may be less of a concern if historical records for this later period can be used as a *terminus post quem*.

CONCLUSIONS

The precision associated with ^{14}C wiggle-matching of tree rings is impacted by the non-monotonic form of the ^{14}C calibration curve, the accuracy and precision of component data sets, and the statistical approach to producing the curve. This paper sought to investigate these factors through the presentation of a new Bayesian spline method for curve construction which was then tested on extant and six new SH data sets (also examining their dendrochronological reliability and pretreatment) for the post-LIA interval AD 1500–1950. The new method of construction allows calculation of component data offsets, permitting identification of laboratory and geographic biases. This enabled us to identify two features of independent interest.

Firstly, we observe the presence of a potential geographical offset at subantarctic Campbell Island. Data from this site shows high offset values probably due to its high latitude in the Southern Ocean and hence we suggest it should be excluded from future SHCal updates. Secondly, measurement of splits of the same wood samples in both Wk and UB

https://doi.org/10.1017/RDC.2019.42 Published online by Cambridge University Press

laboratories provided information on the potential sizes of analytical offsets between laboratories. Our study suggested such laboratory offsets may lie in the region of 12.8 ± 3.9 yr. This implies that high-resolution data sets need to be compiled by at least two different laboratories to mitigate the impact of individual laboratory biases distorting the calibration curves.

In addition to the above, we investigated the effect of pre-treatment methods. The Western Australia Lake Tay data compiled from highly resinous *Callitris columellaris* trees shows some data points which may be influenced by resin translocation across ring boundaries. Further work is required to determine the suitability of these measurements for calibration purposes.

Application of the new calibration method to the 10 suitable SH ^{14}C data sets suggests that individual offset ranges for component data sets, appear to be in the region of ±10 yr. Data sets with individual offsets larger than this need to be carefully assessed before selection for calibration purposes. A wiggle-match of 12 five-year segments from a New Zealand miro palisade post produced similar results using the new method of curve construction (and new data) when compared with OxCal using SHCal13. This is likely due to the unique shape of the post's ^{14}C determinations lying on an inversion of the calibration curve. In general, we expect that the new method of curve construction will provide somewhat wider credible intervals when calibrating objects against it, a desirable feature given recent evidence for possible over-precise and inaccurate wiggle-matching using current calibration curves (Bayliss et al. 2017).

Importantly, simulations using OxCal and the new SH curve suggest that wiggle-matching short sequences (e.g. less than ~60-rings) can however produce accurate wiggle-matches that still have high levels of precision (e.g. ranges of less than ~10 yr) in the AD 1650–1850 interval. Earlier and later time periods in the time interval AD 1500–1950 containing ^{14}C plateaux or repeating structures may produce lower levels of precision, with ranges of 20–30 yr or more.

REFERENCES

Baillie MGL, Pilcher JR. 1973. A simple crossdating program for tree-ring research. Tree-Ring Bulletin 33:7–14.

Bayliss A, Marshall P, Tyers C, Ramsey CB, Cook G, Freeman SP, Griffiths S. 2017. Informing conservation: towards ^{14}C wiggle-matching of short tree-ring sequences from medieval buildings in England. Radiocarbon 59(3):985–1007.

Blackwell PG, Buck CE. 2008. Estimating radiocarbon calibration curves. Bayesian Analysis 3(2):225–248.

Braziunas TF, Fung IY, Stuiver M. 1995. The preindustrial atmospheric $^{14}CO_2$ latitudinal gradient as related to exchanges among atmospheric, oceanic, and terrestrial reservoirs. Global Biogeochemical Cycles 9(4):565–584.

Bronk Ramsey C. 2009. Dealing with outliers and offsets in radiocarbon dating. Radiocarbon 51(3):1023–1045.

Bronk Ramsey C, Staff RA, Bryant CL, Brock F, Kitagawa H, van der Plicht J, Schlolaut G, Marshall MH, Brauer A, Lamb HF, Payne RL. 2012. A complete terrestrial radiocarbon record for 11.2 to 52.8 kyr BP. Science 338(6105):370–374.

Bronk Ramsey C, van der Plicht J, Weninger B. 2001. "Wiggle matching" radiocarbon dates. Radiocarbon 43(2A):381–389.

Capano M, Miramont C, Guibal F, Kromer B, Tuna T, Fagault Y, Bard E. 2018. Wood ^{14}C dating with AixMICADAS: methods and application to tree-ring sequences from the younger dryas event in the Southern French Alps. Radiocarbon 60(1):51–74.

Cullen LE, Grierson PF. 2009. Multi-decadal scale variability in autumn-winter rainfall in south-western Australia since 1655 AD as reconstructed from tree rings of *Callitris columellaris*. Climate Dynamics 33(2–3):433–444.

D'Arrigo RD, Buckley BM, Cook ER, Wagner WS. 1996. Temperature-sensitive tree-ring width chronologies of pink pine (*Halocarpus biformis*)

https://doi.org/10.1017/RDC.2019.42 Published online by Cambridge University Press

from Stewart Island, New Zealand. Palaeogeography, Palaeoclimatology, Palaeoecology 119(3–4):293–300.

Dee MW, Brock F, Harris SA, Ramsey CB, Shortland AJ, Higham TF, Rowland JM. 2010. Investigating the likelihood of a reservoir offset in the radiocarbon record for ancient Egypt. Journal of Archaeological Science 37(4):687–693.

Friedrich M, Remmele S, Kromer B, Hofmann J, Spurk M, Kaiser KF, Orcel C, Küppers M. 2004. The 12, 460-year Hohenheim oak and pine tree-ring chronology from central Europe—a unique annual record for radiocarbon calibration and paleoenvironment reconstructions. Radiocarbon 46(3):1111–1122.

Galimberti M, Ramsey CB, Manning SW. 2004. Wiggle-match dating of tree-ring sequences. Radiocarbon 46(2):917–924.

Grissino-Mayer HD. 2001. Evaluating crossdating accuracy: a manual and tutorial for the computer program COFECHA. Tree-Ring Research 57(2): 205–221.

Heaton TJ, Blackwell PG, Buck CE. 2009. A Bayesian approach to the estimation of radiocarbon calibration curves: the IntCal09 methodology. Radiocarbon 51(4):1151–1164.

Heaton TJ, Blaauw M, Blackwell PG, Ramsey CB, Reimer PJ, Scott ME. 2019 (forthcoming) The IntCal19 approach to radiocarbon calibration curve construction: a new implementation using Bayesian Splines and errors-in-variables. Radiocarbon 62(1).

Hogg AG, McCormac FG, Higham TF, Reimer PJ, Baillie MG, Palmer JG. 2002. High-precision radiocarbon measurements of contemporaneous tree-ring dated wood from the British Isles and New Zealand: AD 1850–950. Radiocarbon 44(3): 633–640.

Hogg A, Palmer J, Boswijk G, Turney C. 2011. High-precision radiocarbon measurements of tree-ring dated wood from New Zealand: 195 BC–AD 995. Radiocarbon 53(3):529–542.

Hogg A, Lowe DJ, Palmer J, Boswijk G, Ramsey CB. 2012. Revised calendar date for the Taupo eruption derived by ^{14}C wiggle-matching using a New Zealand kauri ^{14}C calibration data set. The Holocene 22(4):439–449.

Hogg AG, Hua Q, Blackwell PG, Niu M, Buck CE, Guilderson TP, Heaton TJ, Palmer JG, Reimer PJ, Reimer RW, Turney CS. 2013a. SHCal13 Southern Hemisphere calibration, 0–50,000 years cal BP. Radiocarbon 55(4):1889–1903.

Hogg A, Turney C, Palmer J, Southon J, Kromer B, Ramsey CB, Boswijk G, Fenwick P, Noronha A, Staff R, Friedrich M. 2013b. The New Zealand kauri (*Agathis Australis*) research project: a radiocarbon dating intercomparison of younger dryas wood and implications for IntCal13. Radiocarbon 55(4):2035–2048.

Hogg A, Southon J, Turney C, Palmer J, Ramsey CB, Fenwick P, Boswijk G, Büntgen U, Friedrich M, Helle G, Hughen K. 2016. Decadally resolved lateglacial radiocarbon evidence from New Zealand kauri. Radiocarbon 58(4):709–733.

Hogg A, Gumbley W, Boswijk G, Petchey F, Southon J, Anderson A, Roa T, Donaldson L. 2017. The first accurate and precise calendar dating of New Zealand Māori Pā, using Otāhau Pā as a case study. Journal of Archaeological Science: reports 12:124–133.

Holmes RL. 1983. Computer-assisted quality control in tree-ring dating and measurement. Tree-Ring Bulletin 43:69–78.

Hong W, Park JH, Park G, Sung KS, Park WK, Lee JG. 2013. Regional offset of radiocarbon concentration and its variation in the Korean atmosphere from AD 1650–1850. Radiocarbon 55(2):753–762.

Hoper ST, McCormac FG, Hogg AG, Higham TF, Head M. 1998. Evaluation of wood pretreatments on oak and cedar. Radiocarbon 40(1):45–50.

Hua Q, Barbetti M, Zoppi U, Fink D, Watanasak M, Jacobsen GE. 2004. Radiocarbon in tropical tree rings during the little ice age. Nuclear Instruments and Methods in Physics Research B 223:489–494.

Kromer B, Manning SW, Kuniholm PI, Newton MW, Spurk M, Levin I. 2001. Regional $^{14}CO_2$ offsets in the troposphere: magnitude, mechanisms, and consequences. Science 294(5551):2529–2532.

Manning SW, Kromer B, Kuniholm PI, Newton MW. 2001. Anatolian tree rings and a new chronology for the east Mediterranean Bronze-Iron Ages. Science 294(5551):2532–2535.

Manning SW, Höflmayer F, Moeller N, Dee MW, Ramsey CB, Fleitmann D, Higham T, Kutschera W, Wild EM. 2014. Dating the Thera (Santorini) eruption: archaeological and scientific evidence supporting a high chronology. Antiquity 88(342):1164–1179.

McCormac FG, Baillie MG, Pilcher JR, Kalin RM. 1995. Location-dependent differences in the ^{14}C content of wood. Radiocarbon 37(2):395–407.

McCormac FG, Hogg AG, Higham TF, Lynch Stieglitz J, Broecker WS, Baillie MG, Palmer JG, Xiong L, Pilcher JR, Brown DS, Hoper ST. 1998. Temporal variation in the interhemispheric ^{14}C offset. Geophysical Research Letters 25(9): 1321–1324.

McCormac FG, Reimer PJ, Hogg AG, Higham TF, Baillie MG, Palmer J, Stuiver M. 2002. Calibration of the radiocarbon time scale for the Southern Hemisphere: AD 1850–950. Radiocarbon 44(3):641–651.

Nakamura T, Masuda K, Miyake F, Nagaya K, Yoshimitsu T. 2013. Radiocarbon ages of annual rings from Japanese wood: evident age offset based on IntCal09. Radiocarbon 55(2):763–770.

Niu M, Heaton TJ, Blackwell PG, Buck CE. 2013. The Bayesian approach to radiocarbon calibration curve estimation: the IntCal13, Marine13, and SHCal13 methodologies. Radiocarbon 55(4):1905–1922.

https://doi.org/10.1017/RDC.2019.42 Published online by Cambridge University Press

Palmer JG, Xiong L. 2004. New Zealand climate over the last 500 years reconstructed from *Libocedrus bidwillii* Hook. f. tree-ring chronologies. The Holocene 14(2):282–289.

Palmer JG, Turney CSM, Hogg AG, Hilliam N, Watson M, van Sebille E, Cowie W, Jones R, Petchey F. 2014. The discovery of New Zealand's oldest shipwreck—possible evidence of further Dutch exploration of the South Pacific. Journal of Archaeological Science 42:435–441.

Palmer JG, Cook ER, Turney CS, Allen K, Fenwick P, Cook BI, O'Donnell A, Lough J, Grierson P, Baker P. 2015. Drought variability in the eastern Australia and New Zealand summer drought atlas (ANZDA, CE 1500–2012) modulated by the Interdecadal Pacific Oscillation. Environmental Research Letters 10(12):124002.

Park J, Southon J, Fahrni S, Creasman PP, Mewaldt R. 2017. Relationship between solar activity and $\Delta^{14}C$ peaks in AD 775, AD 994, and 660 BC. Radiocarbon 59(4):1147–1156.

Pearson CL, Brewer PW, Brown D, Heaton TJ, Hodgins GWL, Jull AJT, Lange T, Salzer MW. 2018. Annual radiocarbon record indicates 16th century BCE date for the Thera eruption. Science Advances 4:eaar8241.

Reimer PJ, Bard E, Bayliss A, Beck JW, Blackwell PG, Bronk Ramsey C, Brown DM, Buck CE, Edwards RL, Friedrich M, Grootes PM, Guilderson TP, Haflidason H, Hajdas I, Hatté C, Heaton TJ, Hogg AG, Hughen KA, Kaiser KF, Kromer B, Manning SW, Reimer RW, Richards DA, Scott EM, Southon JR, Turney CSM, van der Plicht J. 2013a. Selection and treatment of data for radiocarbon calibration: an update to the International Calibration (IntCal) criteria. Radiocarbon 55(4):1923–1945.

Reimer P, Bard E, Bayliss A, Beck W, Blackwell P, Bronk Ramsey C, Buck C, Cheng H, Edwards L, Friedrich M, Grootes P, Guilderson T, Haflidason H, Hajdas I, Hatté C, Heaton T, Hoffmann D, Hogg A, Hughen K, Kaiser F, Kromer B, Manning S, Niu M, Reimer R, Richards D, Scott M, Southon J, Staff R, Turney C, van der Plicht J. 2013b. IntCal13 and Marine13 radiocarbon age calibration curves 0–50,000 years cal BP. Radiocarbon 55(4):1869–1887.

Rodgers KB, Mikaloff-Fletcher SE, Bianchi D, Beaulieu C, Galbraith ED, Gnanadesikan A, Hogg AG, Iudicone D, Lintner BR, Naegler T, Reimer PJ. 2011. Interhemispheric gradient of atmospheric radiocarbon reveals natural variability of Southern Ocean winds. Climate of the Past 7(4):1123–1138.

Scott EM, Naysmith P, Cook GT. 2017. Why do we need ^{14}C inter-comparisons?: the Glasgow-^{14}C inter-comparison series, a reflection over 30 years. Quaternary Geochronology 43:72–82.

Southon JR, Magana AL. 2010. A comparison of cellulose extraction and ABA pretreatment methods for AMS ^{14}C dating of ancient wood. Radiocarbon 52(3):1371–1379.

Southon J, Noronha AL, Cheng H, Edwards RL, Wang Y. 2012. A high-resolution record of atmospheric ^{14}C based on Hulu Cave speleothem H82. Quaternary Science Reviews 33:32–41.

Stuiver M, Braziunas TF. 1998. Anthropogenic and solar components of hemispheric ^{14}C. Geophysical Research Letters 25(3):329–332.

Taylor R, Bar-Yosef O. 2014. Radiocarbon Dating: an Archaeological Perspective. 2nd Edition. New York: Routledge.

Turney CSM, Fogwill CJ, Palmer JG, van Sebille E, Thomas Z, McGlone M, Richardson S, Wilmshurst JM, Fenwick P, Zunz V, Goosse H, Wilson KJ, Carter L, Lipson M, Jones RT, Harsch M, Clark G, Marzinelli E, Rogers T, Rainsley E, Ciasto L, Waterman S, Thomas ER, Visbeck M. 2017. Tropical forcing of increased Southern Ocean climate variability revealed by a 140-year subantarctic temperature reconstruction. Climate of the Past 13:231–248.

Turney CS, Palmer J, Hogg A, Fogwill CJ, Jones RT, Bronk Ramsey C, Fenwick P, Grierson P, Wilmshurst J, O'Donnell A, Thomas ZA. 2016. Multidecadal variations in Southern Hemisphere atmospheric ^{14}C: evidence against a Southern Ocean sink at the end of the Little Ice Age CO_2 anomaly. Global Biogeochemical Cycles 30(2):211–218.

Turney CS, Palmer J, Maslin MA, Hogg A, Fogwill CJ, Southon J, Fenwick P, Helle G, Wilmshurst JM, McGlone M, Ramsey CB. 2018. Global peak in atmospheric radiocarbon provides a potential definition for the onset of the Anthropocene epoch in 1965. Scientific Reports 8(1):3293.

Tyers I. 1997. Dendro for Windows program guide. Report No.: 340. Sheffield (UK): Archaeological Research and Consultancy at University of Sheffield.

Vogel JC, Fuls A, Visser E, Becker B. 1986. Radiocarbon fluctuations during the third millennium BC. Radiocarbon 28(2B):935–938.

Vogel JC, Fuls A, Visser E, Becker B. 1993. Pretoria calibration curve for short-lived samples, 1930–3350 BC. Radiocarbon 35(1):73–85.

Ward GK, Wilson SR. 1978. Procedures for comparing and combining radiocarbon age determinations: a critique. Archaeometry 20(1): 19–31.

Xiong L, Palmer JG. 2000a. Reconstruction of New Zealand temperatures back to AD 1720 using *Libocedrus bidwillii* tree rings. Climatic Change 45(2):339–359.

Xiong L, Palmer JG. 2000b. *Libocedrus bidwillii* tree-ring chronologies in New Zealand. Tree-Ring Bulletin 56:1–16.

https://doi.org/10.1017/RDC.2019.42 Published online by Cambridge University Press